ACOUSTICS EMISSION DIAGNOSTICS OF BRIDGES

Valentin Skalsky[1,a], Zinovii Nazarchuk[1], Denys RUDAVSKYY[1,b] and Oleg Sergiyenko[1]

[1]Karpenko Physico-Mechanical Institute of National Academy of Sciences of Ukraine

5, Naukova str., Lvov, 79060, Ukraine

[a]skal@ipm.lviv.ua, [b]denrud@ipm.lviv.ua

Keywords: bridge, beam, static and dynamic loading, acoustic emission, measuring system.

Abstract. The paper describes the methodology of acoustic emission (AE) diagnostics of the metal steel beam of the bridge over the Dniester River. The bridge was built in the early twentieth century and renovated in 1956. The bridge length is 261,9 m. The main bearing structures of the bridge are continuous welded beams. For diagnosing the technical condition of beams, AE methodology developed in the Physico-Mechanical Institute of NAS of Ukraine was applied. It consists in the preliminary study of specific character of elastic waves propagation in materials the bridge made, and the application of the developed portable eight channels AE measurement system SKOP-8. The tests were conducted under static and dynamic loading. Linear and planar location techniques were applied in order to identify sites of nucleation and development of fracture. By using AE data obtained in full-scale tests, the analysis of technical state of bearing structures of the bridge was performed and proposals concerning their further operation were made.

Method of acoustic emission (AE) became available for commercial use over 40 years ago. Its application is increased greatly in various industries around the world. Initially, it was tested in fields, where existing methods of non-destructive testing were nonperforming or where it promised economic benefits. Late 1970 - early 1980, when AE researches in academic and industrial centres of the USA, Europe, Japan started up, qualitative changes in approaches to use this method occurred [1]. Academic researches focused on rare occasions of establishing relationships between AE signals shapes (AE parameters) and the sources characteristics or mechanisms of fracture. At the same time, AE researches of industrial structures accumulated amount of data that not only enabled establishing zone location of sources, but also demonstrated relationships between AE signals and fracture mechanisms, corrosion processes, technical state of building elements, showing features of elastic waves generated in composite structures and their elements that operated at elevated pressure. The progress of computer technology made possible the efficient analysis of stored data, creating preconditions for manufacturing specialized AE equipment designed for operation at power plants, refineries, chemical plants, pipelines, airplanes, etc.

The structures of the successful AE diagnostics were compressed gas tanks, storage tanks for liquids, concrete waste storages, reinforced concrete and steel bridges, pipelines for oil and gas, off-shore platforms, ropes, elements of power equipment (pipelines of boilers, fuel rod ferrules, heat exchangers, high pressure tanks), airplane components (fuselage skin, turbine engine blades, protective coating of combustion chamber), etc.

Problems of application of AE method are worsened when the structure has a complex geometry, weld and other types of connections. Therefore, it remains urgent to develop new and improve existing means of processing the information, detected by transducers, whose data processing rate and

reliability is still insufficient for large-scale implementation of AE diagnostics of various test units. Effective application of this method depends greatly on the modes of results presentation, automated data processing that would enable to reduce the number of staff, decrease the influence of "human factor". These difficulties associated with unknown dependencies of parameters of AE signals on the nature of the origin and propagation of material fracture, especially taking into account that the various fracture mechanisms are still not studied completely.

Despite these difficulties, AE diagnostics is steadily gaining its proper place among other methods of non-destructive testing. Today, when many metal consuming, technologically sophisticated and environmentally dangerous structures exhausted their life, is extremely urgent need to establish their technical condition and remaining life. AE method successfully performs this function. Examples of its successful application presented in this paper.

Acoustic emission signals caused by local subcritical crack growth. For estimation of AE signals radiation caused by subcritical crack growth at local areas of its front, we consider an elastic half-space with a flat mode I macrocrack bounded by a smooth contour *L* (see Fig. 1).

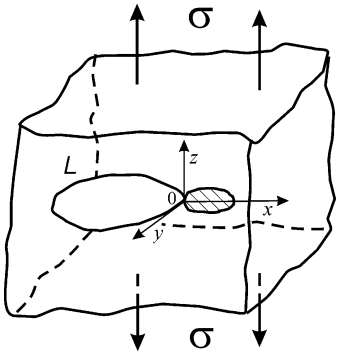

Fig. 1. The schematic of local growth of internal crack.

Let at the time t=0 in local area, where stresses (or deformations) achieve certain critical value, due to application of external tensile forces to a body, a microcrack nucleates closely a contour of this macrocrack . As a result of unloading of the surfaces of this newly formed microcrack from an initial level down to zero, elastic waves are radiated. They reach the inspected object surface and can be detected by an AE transducer.

For simplification of the problem, we replace this microcrack with a penny-shaped mode I crack equal to it by the area. Let us suppose also, that radius of this penny-shaped microcrack is much less than the radius of macrocrack contour curvature. In this case, instead of the above-mentioned problem we may to consider the problem of a sudden nucleation of a penny-shaped microcrack near the front of a through semi-infinite macrocrack.

Let us estimate resulting components of the dynamic displacement field. Consider now dynamic problem of growth of a semi-infinite through crack in homogeneous isotropic elastic body. For this problem the following angular dependencies $\Phi_i^h(\beta)$ of radiation field were obtained in [2] (β is the angle in polar coordinate system $Or\beta$, which origin coincides with this semi-infinite through crack tip). They correspond to longitudinal and transverse waves that are valid for the wave front region.

$$\Phi_i^h(\beta) = V_i(\beta) C_i(\beta) P_i(\beta),\ i = 1,2. \tag{1}$$

Here the functions

$$V_i(\beta) = 1/(1 - c_c/c_i \cos\beta), \tag{2}$$

describe the change in angular dependence of radiation caused by the crack edge propagation with velocity c_c for a component of longitudinal (i=1) and shear (i=2) waves. Functions

$$C_i(\beta) = \frac{\sqrt{1 + c_1/c_i \cos\beta}}{(1 + c_R/c_i \cos\beta) K\_(-s_i \cos\beta)}, \tag{3}$$

where $$K_{\pm}(\eta)=\exp\left\{-\frac{1}{\pi}\int_{s_1}^{s_2}\frac{g(z)dz}{z\pm\eta}\right\},\ s_i=1/c_i\,, \tag{4}$$

$$g(z)=\tan^{-1}\left\{4z^2\sqrt{z^2-s_1^2}\sqrt{s_2^2-z^2}\left(s^2-2z^2\right)^{-2}\right\} \tag{5}$$

determine the influence of the free surface of a semi-infinite crack on the angular distribution of radiation.

Functions $$P_1(\beta)=1-2(c_2/c_1)^2\cos^2\beta;\ P_2(\beta)=\sin 2\beta \tag{6}$$

determine the angular dependencies of maximum values of the displacement vector module at the fronts of longitudinal and shear waves radiated by the edge of this crack; c_R is the Raleigh wave velocity.

Previously we discussed the problem of instant formation of penny-shaped crack of mode I [3]. We supposed that a penny-shaped crack of radius r_0 nucleated when the tensile stresses in certain region of elastic body achieve the certain critical value σ_0 (the integral characteristics of material breaking strength). The crack formation is accompanied by the instant drop of normal stresses on its surfaces from an initial level σ_0 to zero.

For estimation of the maximum values of the displacement vector module the following approximation expressions are given:

$$u_{\max}\big|_{c_i}=\delta_i\frac{\sigma_0\Phi_i^{(d)}(\theta)r_0^2}{\rho c_1^2 R}, \tag{7}$$

where i = 1 corresponds to longitudinal wave and i = 2 to shear wave, the parameters of approximation δ_1=0.452, δ_2=0.832 were obtained by the least squares method, R – is the distance from the crack center to a view point.

Angular dependencies of peak values of the displacement vector module take the form

$$\Phi_1^{(d)}(\theta)=\left(1-2\varepsilon^2\cos^2\theta\right)\left(1+\chi_1\cos^2\theta\right)^{-1/2} \tag{8}$$

$$\Phi_2^{(d)}(\theta)=\left|\sin 2\theta\right|\left(1+\chi_2\cos^2\theta\right)^{-1/2}, \tag{9}$$

for the longitudinal and shear wave, respectively, χ_1 and χ_2 are the parameters of approximation. Their numerical values χ_1=0.68 and χ_2=2.69 at ε=0.535 and ν=0.32 were obtained also by the least squares method, ν - is the Poisson's ratio, $\varepsilon = c_2/c_1$, $c_1=\sqrt{(\lambda+2\mu)/\rho}$ is the velocity of longitudinal wave, $c_2=\sqrt{\mu/\rho}$ is the velocity of shear wave, λ, μ are Lame's constants, ρ is the material density.

The comparison of expression (6) with the dependencies (8) and (9) for case of a penny-shaped crack nucleation shows their similarity. So, if the cause of elastic waves radiation is the nucleation of a penny-shaped microcrack closely to the contour of a macrocrack, then the influence of the free surfaces of the macrocrack on a displacement field caused by formation of this penny-shaped crack can be estimated using dependence (3).

Therefore, we express a radiation field at a distance significantly larger then the microcrack radius as a product of displacement components for instant nucleation of a penny-shaped crack in elastic body (see Ref. [3]) by functions $C_i(\beta)$ defined in eq. (3) accounting for the effect of a free surface.

In spherical coordinate system $OR\theta\varphi$, which origin coincides with a center of a penny-shaped crack, the components of a displacement vector at distances $R>>r_0$ can be written as follows:

$$u_R(\mathbf{R},t)=C_1(\beta)u_R^{(d)}(\mathbf{R},t),\ \ u_\theta(\mathbf{R},t)=C_2(\beta)u_\theta^{(d)}(\mathbf{R},t), \tag{10}$$

where functions $u_R^{(d)}(\mathbf{R},t)$ and $u_\theta^{(d)}(\mathbf{R},t)$ are determined in [3],

$$\cos\beta=\left(\cos\theta\sin\varphi+\delta\right)\left[\left(\cos\theta\sin\varphi+\delta\right)^2+\sin^2\theta\right]^{-1/2}, \tag{11}$$

$\delta=\Delta/R$, Δ is the distance between the center of a penny-shaped crack and the edge of a semi-infinite crack.

For large R $\delta \to 0$. The components u_R and u_θ expressed by equations (10) have the same time dependence as appropriate components $u_R^{(d)}$ and $u_\theta^{(d)}$.

It follows from dependencies (10) that the magnitude of displacements at the front of a radiated longitudinal wave is proportional to r_0^2:

$$u_{\max}\Big|_{c_1} = \frac{\delta_1 \sigma_0 r_0^2}{\rho c_1^2 R} \Phi_1^{(d)}(\theta) C_1(\beta), \qquad (12)$$

i.e. to the area of a nucleated defect.

Let us go back to consideration of the problem on a microdefect of area *S* nucleation in the vicinity of the internal macrocrack contour. Assuming that *S* is equal to the area of a microcrack and that amplitude *A* of AE signal is proportional to magnitude of displacement at the front of longitudinal wave, we find

$$A = \lambda S R^{-1} \Phi_1^{(d)}(\theta) C_1(\beta), \qquad (13)$$

where $\lambda = \lambda_0 \lambda_1$ and λ_0 is a proportionality factor between electrical signals in the output of AET and maximum values of displacements at the front of longitudinal wave, $\lambda_1 = \delta_1 \sigma_0 / (\pi \rho c_1^2)$. If during local growth of an internal crack in the vicinity of its contour *N* of such microdefects were formed then the total area of internal macrocrack growth

$$\Delta S = \sum_{k=1}^{N} b A_k \,, \quad \text{where } b \text{ is a proportionality factor.} \qquad (14)$$

Thus, as follows from dependencies (14), the amplitudes of AE signals caused by the internal flat crack growth in local areas of its front are proportional to the total growth area. Such a form of relationship between *A* and *S* was confirmed experimentally [15;4].

Specification of the research subject. The bridge over the Dniester River was built in the early twentieth century and renovated in 1956. It consists of five baulks. The bridge scheme is 5 × 47,5 m. Its total length is 261,9 m. The bridge roadway clearance is H – 6,8 + 2 × 1,5 m (see Fig. 2). Coastal and stream baulks 1 – 2, 2 – 3, 3 – 4 consist of one continuous welded section, which has in its cross-section two double-tee beams of welded metal type, the distance between their axles is 5.0 m. The beams are strengthened the entire length of two-sided vertical and horizontal ribs. Metal structures are made of steel M-16S.

a)

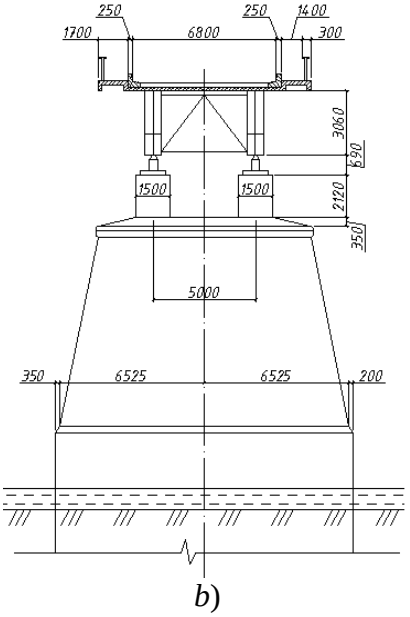

b)

Fig. 2. General view of the bridge (*a*) and its cross-section (*b*)

Dimensions of metal beams: height is 3,06 m, width of the upper beam flange is 600 – 400 mm, width of the lower beam flange is 600 – 400 mm, thickness of the upper beam flange is 15 – 40 mm, thickness of the bottom beam flange is 20 – 40 mm. Beams are connected to the reinforced concrete slab of the bridge roadway with stops made of L-squares of 100×100×10 mm.
Lateral stiffness of baulks are provided by cross connections of triangular system with spacers. Lower longitudinal cross-system connections are made at the lower ring of the beam with holders that were placed every 8,5 m

Methodology and testing program.

Measuring tools. Two 8-channel AE systems SKOP-8 [2;5] developed in the Karpenko Physico-Mechanical Institute of National Academy of Sciences of Ukraine were used for AE diagnostics of the bridge baulks. The system SKOP-8 (see Fig. 3) provides the selection, recording and preliminary processing of AE signals, their storage in a PC of notebook type for the subsequent data post processing, visualization of results in real time etc.

Fig. 3. AE information-measuring system SKOP-8: 1 is the gage unit; 2 is the circuit board, 3 is the preamplifier, 4 is the slot of the gage unit, 5 is the notebook.

The developed software allows us to locate AE sources, display AE locations together with the draft of tested structure and waveforms of AE events. The system also allows finding the following characteristics of AE signal: AE waveform, frequency spectrum, envelope amplitude, cumulative count, the sum of envelope amplitudes, the count rate, rise time of the pulse, its duration etc. The system records information from the eight independent signal channels. At the time when arrived signal in any of eight channels exceeds the threshold noise level, recording of AE signals in digital form in all channels starts with precise start time value recording for each channel. The obtained information is visualized on PC display in real time.
All AE testing data are recorded on the hard disk of PC for their analysis and processing. PC controls the AE information-measurement system. Using the developed software one can select the number of measuring channels, sampling rate of signals, amplification factors of AE channels and parametric channels, bandwidth and threshold level. Power system voltage is 5V, it supplied through the notebook USB port.

Specifications of the AE system:

Number of input AE channels: 8
Number of input channels for additional information..... 3
THD per AE channel ..... ≤ 2%;
Difference in transfer ratios of channels ..... ≤ 3%;
Frequency range of AE channel.....75 kHz ... 1000 kHz;
Cut-off frequency of high pass filter …….....75, 100, 200, 300 kHz;
Cut-off frequency low pass filter …….....0.4; 0.6, 0.8, 1 MHz;
Input resistance of preamplifier ..... ≥ 1 MΩ;

Bit resolution of analog-to-digital converter ..... 12 bits;
Sampling period of AE channels ..... ≤ 62.5 ns;
Sampling period for low frequency channels ..... 10 ... 640 ms;
Error ..... ≤ 1 digit of analog-to-digital converter

Bridge static loading test. We conducted AE diagnostics of the beam according to the following static loading diagrams:
Diagram 1: formation of maximum stress in the beam at the upper side of the baulk 0-1 by non-symmetric load with respect to the axis of the bridge road using six trucks;
Diagram 2: formation of maximum stress in the beam at the upper side over bridge pillar # 1 by non-symmetric load with respect to the axis of the bridge road using eight trucks;
Diagram 3: formation of maximum stress in the beam at the upper side of the baulk 2-3 by non-symmetric load with respect to the axis of the bridge road using eight trucks;
Diagram 4: formation of maximum stress in the beam at the upper side over bridge pillar # 2 by non-symmetric load with respect to the axis of the bridge road using eight trucks;
Bridge dynamic loading test. During dynamic testing of the bridge, the following loading diagrams were implemented:
Diagram 1d: driving of the truck over the bridge. The truck weight was 0.25 MN, the speed was 10 km/h
Diagram 2d: The truck speed was 20 km / h
Diagram 3d: The truck speed was 40 km / h.
Layout chart of AE sensors. AE sensors at the tested bridge were located according to a linear location layout chart. They were mounted at the studied baulk, and the maximum distance between them was determined by the method described in paper [6] (see Fig. 3;4). Taking into account AE elastic waves attenuation in the tested structure the distance between AE sensors was selected within the range 0,93 ... 1,67 m with the same geometry for every bridge span.

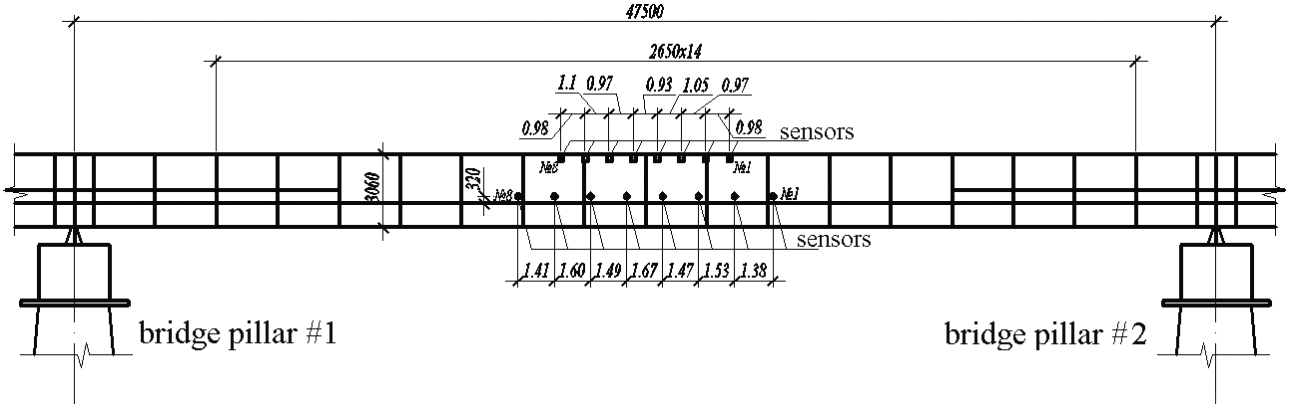

Fig. 4. Example of AE sensor placement in the baulk 2-3.

These optimal layout charts of AE sensors were selected to evaluate the beam operation in its most tensile zones employing the highest sensitivity of the AE instrumentation [7].
The results of the baulks investigation and their interpretation. Some results of the bridge testing under static and dynamic loading are given in Fig. 5 – 7.

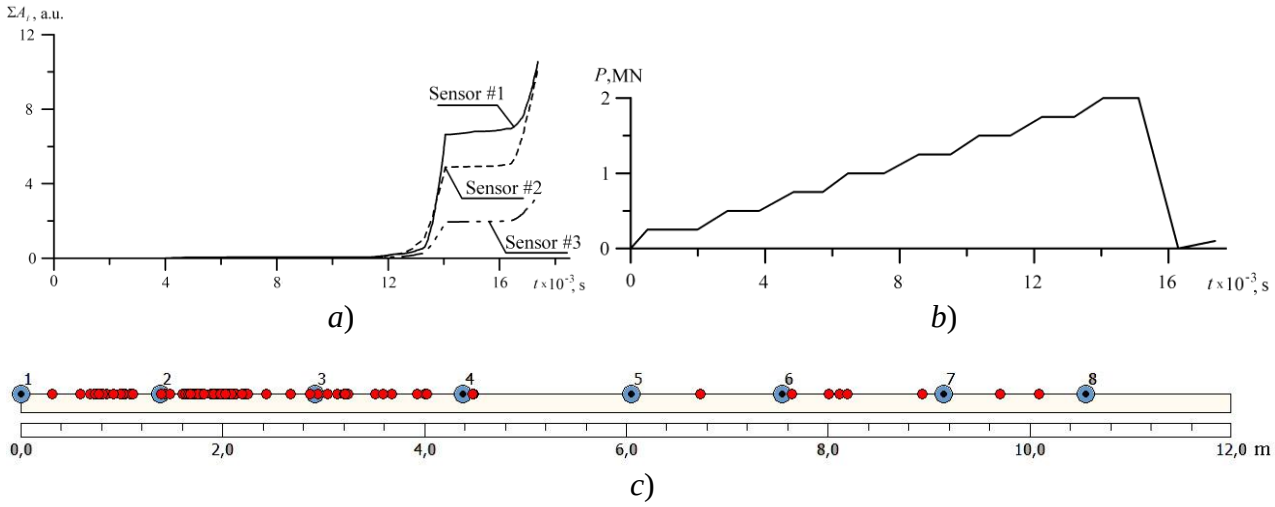

Fig. 5. Time *t* variation of the sum of AE amplitudes ΣA_i (*a*) and load *P* (*b*); 1-8 are the AE sensors located at the upper ring of the beam, red points are the AE source locations under static loading of the 2-3 baulk according to the loading *diagram 2* (*c*).

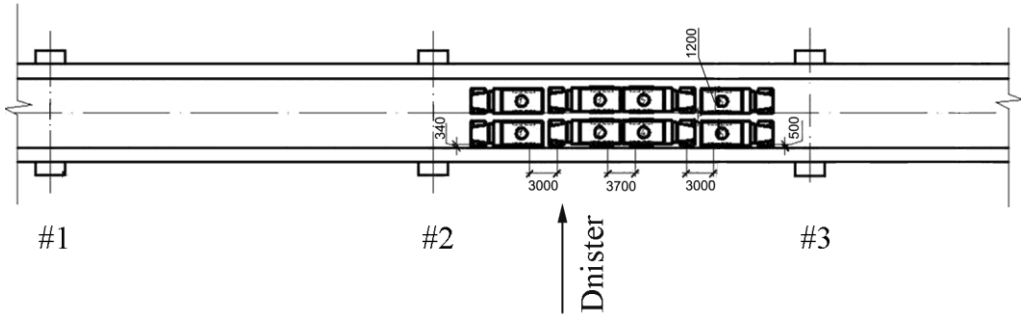

Fig. 6. Test diagram of the baulk 2-3 by non-symmetric loading with respect to the axis of the bridge road using eight trucks of total weight of 2 MN: #1 – #3 its bridge pillars.

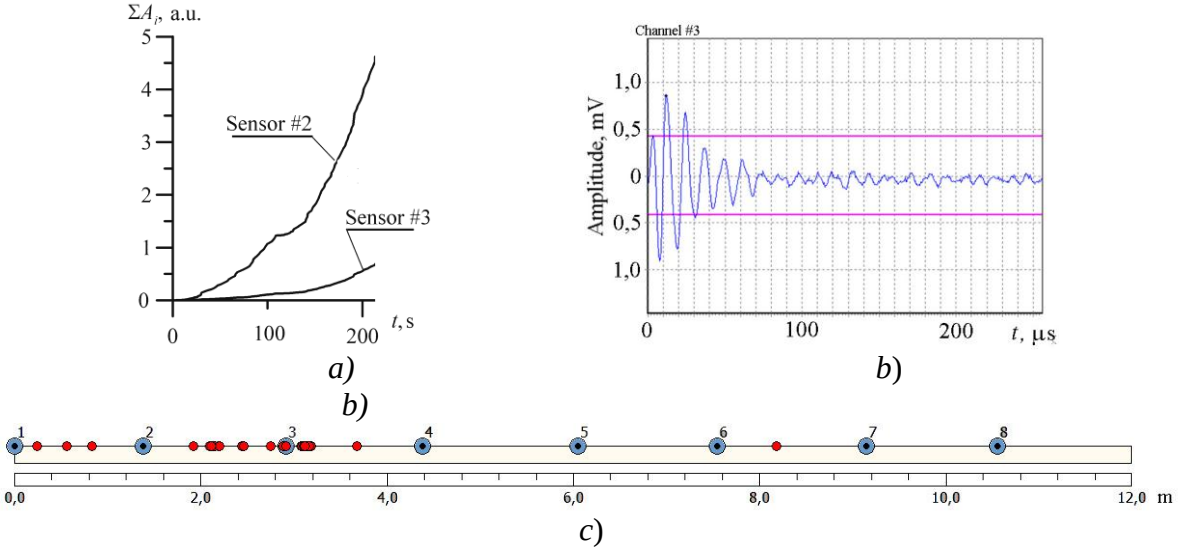

Fig. 7. Time *t* variation of the sum of AE amplitudes of ΣA_i (*a*); characteristic AE signal waveform under dynamic loading of the 2-3 baulk according to the loading *diagram 1d* (*b*); 1-8 are the AE sensors located at the upper ring of the beam, red points are the AE source locations (*c*).

Thus, during static and dynamic loading of the bridge baulks under these loading diagrams maximum amplitudes of AE signals did not exceed the critical level of 1.0 mV. During tensile loading of compact specimens sized 220x280x10 mm we found that this level corresponded to nucleation and development of fracture in this steel. In order to detect an incremental grow of the crack we used thermal staining and impact fracture of the embrittled samples [3,8]. Thus, the AE signals which we recorded at the loaded bridge were probably emitted from contact zone of the reinforced concrete slab of the bridge road with the top- fillet of the metal beam.
These circumstances allowed us to suppose that there were no most dangerous crack-like defects in the bridge and it can operate in the future as usual. In order to prevent dangerous cracks formation in supporting beams of the bridge, we recommend passing trucks weighing more than 0,1 MN one by one (only one truck on the bridge).

Conclusions

Dynamic loading of the bridge by large-tonnage vehicles more significantly influences the processes of AE signals generation in comparison with a static loading case.
AE method is highly sensitive tools for diagnostics of technical condition of load-bearing elements of bridge structures. Application of AE multichannel measuring systems effectively provides monitoring of bridge structures and allows preventing their unexpected failure.

References

[1] Acoustic Emission. Standards and Technology Update (1999): ASTM STP 1353, Sotirios J. Vahaviolos editor, ASTM.

[2] J.D. Achenbach and J.G. Harris, Acoustic emission from a brief crack propagation event. *J. Appl. Mech.* (1979), **46** (1): 107 - 112.

[3] Andreykiv O.Ye., Lysak M.V., Serhienko O.M., Skalsky V.R. Analysis of acoustic emission caused by internal crack. *Eng. Fract. Mech.* 68 (2001), 1317-1333

[4] W.W. Gerberich, D.G. Alteridge and J.F. Lessar, Acoustic emission investigation of microscopic ductile fracture. *Met. Trans. A.* (1975), **6A** (2): 797 - 801.

[5] Nazarchuk Z.T., Skalsky V.R. Acoustic emission diagnostics of structural elements. Engineering handbook. Vol. 3 (2009). Equipment and its employment in acoustic emission studies.

[6] Nazarchuk Z.T., Skalsky V.R. Acoustic emission diagnostics of structural elements. Engineering handbook. Vol. 2 (2009). Methodology of acoustic-emission diagnostics

[7] Skalskyi V.R., Koval P.M. Some methodological aspects of application of acoustic emission (2007).

[8] Skal’s’kyj V.R., Serhienko O.V., Selivonchyk N.V., Oliyarnyk B.O., Plakhtii R.M. Acoustic emission analysis of the stages of subcritical development of cracks in materials. *Materials Science* 43 (2007), № 4, 543.